Toward Robust Passivity: A Passive Control Implementation Structure for Mechanical Teleoperators *

Dongjun Lee and Perry Y. Li *
Department of Mechanical Engineering, University of Minnesota,
111 Church St. SE, Minneapolis MN 55455. {djlee,pli}@me.umn.edu

Abstract

In previous papers, a passive control implementation structure is proposed for mechanical systems interacting with physical environments. The proposed implementation structure enforces robust passivity of the closed-loop system, i.e. passivity is ensured in the presence of inaccurate force sensing and model uncertainties. In this paper, we conduct experiments to validate and demonstrate this robust passivity property of the passive control implementation structure in the context of mechanical teleoperator control. The experiments show that the implementation structure indeed ensures passivity of the closed-loop teleoperator by limiting the amount of energy generated by the control action even in the presence of model uncertainties and master-slave force sensings corrupted with time-delays. Thus, safety and interaction stability of the closed-loop teleoperator are substantially enhanced.

1. Introduction

Energetic passivity of the teleoperator has been widely utilized to ensure interaction stability and safety of human operators and objects in the slave environments. First introduced for teleoperation in [1], time-domain passivity now receives attention of many researchers again due to its capability to deal with nonlinear teleoperator / haptic devices and nonlinear virtual environments [2], [3].

A control approach is proposed in [4, 5] for nonlinear mechanical teleoperator. This control law achieves master-slave configuration coordination by feedforward canceling mismatched forcings. Inertia scaling (with a user-specified scaling factor) of the coordinated teleoperator is also achieved to adjust bandwidth of force feedback according to a task objective (e.g. larger for hammering or smaller for delicate tasks). Since the feedforward cancellation and the inertia scaling tend to violate passivity, the proposed control scheme utilizes a special implementation structure to enforce passivity, which is originally proposed in [6] and later adopted in [7, 8, 9, 10, 11]. The passive implementation structure utilizes energy stored in fictitious passive energy storages to generate possibly non-passive control actions. This implementation structure ensures that the controller itself is passive, since the amount of energy generated by the control actions is bounded by the stored energy in the passive energy storages. This, in turn, implies passivity of the closed-loop teleoperator, since it is an interconnection of the controller and the (energetically conservative) open-loop mechanical systems (master and slave robots).

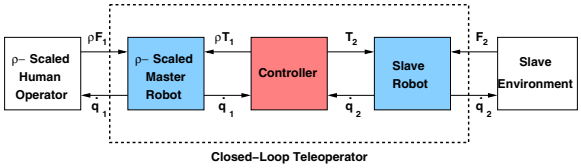

Figure 1. The closed-loop teleoperator is a two-port system. The power scaling is naturally incorporated as the scaled master robot and the human operator with the factor $\rho > 0$.

The advantage of the passive control implementation structure is that passivity of the closed-loop system is enforced *robustly*, i.e. passivity is ensured regardless of inaccurate force measurement and model uncertainties. In [4, 5], this robust passivity was proved theoretically for mechanical teleoperators. In this paper, this robust passivity property of the passive control implementation structure is **experimentally** validated. In particular, to verify that the implementation structure indeed ensures robust passivity, we impose large time-delays (35, 350ms) on force sensing during hard contacts with an aluminum wall of stiffness 33kN/m under the sampling rate of 500Hz.

The rest of the paper is organized as follows. Section 2

*⋆ : Corresponding author. Research supported by National Science Foundation under grant CMS-9870013 and Doctoral Dissertation Fellowship of University of Minnesota.

Proceedings of the11th Symposium on Haptic Interfaces for Virtual Environment and Teleoperator Systems (HAPTICS'03)
0-7695-1890-7/03 $17.00 © 2003 IEEE

introduces passivity of mechanical teleoperators and power scaling. The passive control implementation structure is presented in section 3. Experiments to verify robust passivity are given in section 4 for mechanical teleoperators and section 5 contains some concluding remarks. Appendix contains the control scheme proposed in [4]-[5], which is used for the experiments.

2. Mechanical Teleoperators and Passivity

We consider a 2n-DOF nonlinear teleoperator consisting of a n-DOF master and a n-DOF slave robots:

$$\rho\{\mathbf{M}_1(\mathbf{q}_1)\ddot{\mathbf{q}}_1 + \mathbf{C}_1(\mathbf{q}_1,\dot{\mathbf{q}}_1)\dot{\mathbf{q}}_1 = \mathbf{T}_1 + \mathbf{F}_1\} \quad (1)$$

$$\mathbf{M}_2(\mathbf{q}_2)\ddot{\mathbf{q}}_2 + \mathbf{C}_2(\mathbf{q}_2,\dot{\mathbf{q}}_2)\dot{\mathbf{q}}_2 = \mathbf{T}_2 + \mathbf{F}_2 \quad (2)$$

where ρ is a user-specified power scaling factor and $(\mathbf{q}_1,\mathbf{q}_2)$, $(\mathbf{T}_1,\mathbf{T}_2)$, $(\mathbf{F}_1,\mathbf{F}_2)$ are the configurations, the control commands from actuators, and the environmental forces for the master and the slave robots, respectively. Here, $\mathbf{M}_i(\mathbf{q}_i) \in \Re^{n\times n}$ and $\mathbf{C}_i(\mathbf{q}_i,\dot{\mathbf{q}}_i) \in \Re^{n\times n}$ $i = 1,2$ are the (positive-definite and symmetric) inertia matrices and the Coriolis matrices of the master and the slave robots. Both the master and the slave systems are energetically passive with respect to the supply rate $(\mathbf{T}_i + \mathbf{F}_i)^T\dot{\mathbf{q}}_i$ $i = 1,2$, i.e. $\int_0^t[\mathbf{T}_i(\tau) + \mathbf{F}_i(\tau)]^T\dot{\mathbf{q}}_i(\tau)d\tau \geq d^2$ for a scalar d $\forall t \geq 0, \mathbf{T}_i, \mathbf{F}_i$ due to the well-known fact that $\dot{\mathbf{M}}_i(\mathbf{q}_i) - 2\mathbf{C}_i(\mathbf{q}_i,\dot{\mathbf{q}}_i)$ are skew-symmetric.

As shown by figure 1, when $(\mathbf{T}_1,\mathbf{T}_2)$ are determined by a controller, the teleoperator (1)-(2) becomes a two-port system with $(\rho\mathbf{F}_1,\mathbf{F}_2)$ and $(\dot{\mathbf{q}}_1,\dot{\mathbf{q}}_2)$ being the input and the output. Thus, we say that the closed-loop teleoperator is energetically passive with the power scaling ρ if $\exists c \in \Re$ s.t.

$$\int_0^t \underbrace{\rho\cdot\mathbf{F}_1(\tau)^T\dot{\mathbf{q}}_1(\tau)}_{\substack{scaled\\ human\ power}} + \underbrace{\mathbf{F}_2(\tau)^T\dot{\mathbf{q}}_2(\tau)}_{\substack{environment\\ power}} d\tau \geq -c^2, \quad (3)$$

$\forall t \geq 0$. The scaled power in (3) inspires the following definition of scaled kinetic energy for the teleoperator:

$$\kappa_\rho(t) = \frac{\rho}{2}\dot{\mathbf{q}}_1^T\mathbf{M}_1(\mathbf{q}_1)\dot{\mathbf{q}}_1 + \frac{1}{2}\dot{\mathbf{q}}_2^T\mathbf{M}_2(\mathbf{q}_2)\dot{\mathbf{q}}_2 \geq 0. \quad (4)$$

By designing a controller s.t. (3) is enforced, safety and interaction stability of the closed-loop system interacting with environments will be enhanced.

3. Passive Control Implementation Structure

In this section, we present a control implementation structure enforcing passivity of the closed-loop teleoperator (3). The passive control implementation structure utilizes fictitious passive energy storages and energy stored in these storages is used to generate control actions that may require temporary outflow of energy. In this way, the implementation structure ensures that the controller itself is passive, since the amount of energy generated by the control actions is always bounded by the stored energy in the *passive* energy storages. This controller passivity leads into the passivity of the closed-loop mechanical teleoperator which is an interconnection (see figure 1) of the (passive) controller and the (energetically conservative) open-loop mechanical systems (master and slave robots) with compatible supply rates.

First, we design a smooth and positive scalar potential function on the master and slave configurations:

$$V : (\mathbf{q}_1,\mathbf{q}_2) \in \Re^{2n} \mapsto V(\mathbf{q}_1,\mathbf{q}_2) \in \Re^+. \quad (5)$$

The potential function (5) serves as a passive fictitious energy storage. For instance, $V(t)$ can represent the energy stored in a fictitious spring that connects the two robots for regulating coordination error.

Incorporating the potential function (5), the control $(\rho\mathbf{T}_1,\mathbf{T}_2)$ in (1)-(2) can be implemented as:

$$\begin{pmatrix}\rho\mathbf{T}_1\\ \mathbf{T}_2\end{pmatrix} := \underbrace{\Gamma(t)\begin{pmatrix}\dot{\mathbf{q}}_1\\ \dot{\mathbf{q}}_2\end{pmatrix} + \begin{pmatrix}-\frac{\partial V}{\partial \mathbf{q}_1}^T\\ -\frac{\partial V}{\partial \mathbf{q}_2}^T\end{pmatrix}}_{passive} + \begin{pmatrix}\rho\mathbf{T}_1^\star\\ \mathbf{T}_2^\star\end{pmatrix} \quad (6)$$

where $\Gamma(t) \in \Re^{2n\times 2n}$ is a skew-symmetric matrix and

$$\frac{\partial V}{\partial \mathbf{q}_i} := \left[\frac{\partial V}{\partial q_i^1}, \frac{\partial V}{\partial q_i^2}\cdots\frac{\partial V}{\partial q_i^n}\right] \quad (7)$$

with $\mathbf{q}_i = \left[q_i^1, q_i^2, \cdots q_i^n\right]^T$ $(i = 1,2)$. Notice that the control implemented by $\Gamma(t)$ does not generate energy, since the power generated by this control is $[\dot{\mathbf{q}}_1^T,\dot{\mathbf{q}}_2^T]\Gamma(t)\begin{pmatrix}\dot{\mathbf{q}}_1\\ \dot{\mathbf{q}}_2\end{pmatrix} = 0\ \forall t \geq 0$. Thus, the control (6) is inherently passive as long as the controls $(\rho\mathbf{T}_1^\star,\mathbf{T}_2^\star)$ is passive (i.e. it generates only a limited amount of energy outflow).

Some useful controls are not passive (e.g. feedforward cancellation) i.e. they can generate infinite amount of energy outflow so that environments can be damaged severely. We implement these non-passive controls into $(\rho\mathbf{T}_1^\star,\mathbf{T}_2^\star)$. To generate these possibly non-passive controls $(\rho\mathbf{T}_1^\star,\mathbf{T}_2^\star)$ in (6) without violating passivity, we utilize another fictitious passive energy storage having the usual m-DOF flywheel dynamics (simulated in software):

$$\mathbf{M}_f\ddot{\mathbf{x}}_f = \mathbf{T}_f \quad (8)$$

where $\mathbf{M}_f \in \Re^{m\times m}$, $\mathbf{x}_f \in \Re^m$ and $\mathbf{T}_f \in \Re^m$ are the (time-invariant) inertia matrix, the configuration and the coupling torque to be defined. Then, the controls $(\rho\mathbf{T}_1^\star,\mathbf{T}_2^\star)$

are implemented as:

$$\begin{pmatrix} \rho\mathbf{T}_1^\star \\ \mathbf{T}_2^\star \\ \mathbf{T}_f \end{pmatrix} = \mathbf{\Omega}^\star(t) \begin{pmatrix} \dot{\mathbf{q}}_1 \\ \dot{\mathbf{q}}_2 \\ \dot{\mathbf{x}}_f \end{pmatrix}. \quad (9)$$

where $\mathbf{\Omega}^\star(t) \in \Re^{(2n+m)\times(2n+m)}$ is chosen to be negative semi-definite (NSD) in order to limit the amount of energy generated by the controls $(\rho\mathbf{T}_1^\star, \mathbf{T}_2^\star)$.

This implementation structure (6)-(9) ensures that the controller itself is passive (controller passivity). Define the controller storage function $T_c(t) = V(t) + \kappa_f(t)$ where $\kappa_f(t) := \frac{1}{2}\dot{\mathbf{x}}_f^T\mathbf{M}_f\dot{\mathbf{x}}_f$ is the kinetic energy of the flywheel (8). Then, using (6), (8), $\frac{dV(t)}{dt} = \frac{\partial V}{\partial \mathbf{q}_1}\dot{\mathbf{q}}_1 + \frac{\partial V}{\partial \mathbf{q}_2}\dot{\mathbf{q}}_2$, and that $\Gamma(t)$ in (6) is skew-symmetric, we have:

$$\frac{dT_c(t)}{dt} = \mathbf{T}_f^T\dot{\mathbf{x}}_f + \rho\mathbf{T}_1^{\star T}\dot{\mathbf{q}}_1 + \mathbf{T}_2^{\star T}\dot{\mathbf{q}}_2 - \rho\mathbf{T}_1{}^T\dot{\mathbf{q}}_1 - \mathbf{T}_2{}^T\dot{\mathbf{q}}_2.$$

Thus, since $V(t) \geq 0, \kappa_f(t) \geq 0$ and $\mathbf{\Omega}^\star(t)$ in (9) is NSD, by integration of the equality, we have

$$\int_0^t \rho\mathbf{T}_1^T(\tau)\dot{\mathbf{q}}_1(\tau) + \mathbf{T}_2^T(\tau)\dot{\mathbf{q}}_2(\tau)d\tau \leq V(0) + \kappa_f(0), \quad (10)$$

$\forall t \geq 0$. This condition (10) implies that the controller itself is passive (controller passivity), i.e. the energy generated by the controller (LHS of (10)) is bounded by the energy stored in the passive storage elements (the potential field and the flywheel as shown in RHS of (10)).

The controller passivity implies passivity of the closed-loop teleoperator which is an interconnection of the (energetically conservative) open-loop master and slave robots and the controller as shown in figure 1. Since the master and the slave (1)-(2) are energetically conservative (i.e. $\dot{\mathbf{M}}_\star(\mathbf{q}_\star) - 2\mathbf{C}_\star(\mathbf{q}_\star, \dot{\mathbf{q}}_\star)$ is skew-symmetric), we have

$$\frac{d\kappa_\rho(t)}{dt} = \rho[\mathbf{F}_1 + \mathbf{T}_1]^T\dot{\mathbf{q}}_1 + [\mathbf{F}_2 + \mathbf{T}_2]^T\dot{\mathbf{q}}_2 \quad (11)$$

where $\kappa_\rho(t)$ is the scaled kinetic energy of the teleoperator in (4). Thus, if the controller passivity condition (10) holds, the passivity condition for the closed-loop teleoperator (3) follows, since we can get

$$\int_0^t [\rho\mathbf{F}_1^T(\tau)\dot{\mathbf{q}}_1(\tau) + \mathbf{F}_2^T(\tau)\dot{\mathbf{q}}_2(\tau)]d\tau \quad (12)$$
$$\geq -\kappa_\rho(0) - \kappa_f(0) - V(0),$$

$\forall t \geq 0$ by integrating the equality (11) using the controller passivity condition (10) and $\kappa_\rho(t) \geq 0$. Thus, the implementation structure (6) - (9) ensures that the closed-loop teleoperator is passive, i.e. the amount of the energy that can be extracted from the closed-loop teleoperator (LHS of (12)) is always upper-bounded by the energy stored in the fictitious passive energy elements (RHS of (12)).

Figure 2. 2-DOF planar master and slave robots. Each is equipped with a force sensor.

From (8) and (9), it can be shown that

$$\frac{d\kappa_f(t)}{dt} = \mathbf{T}_f^T\dot{\mathbf{x}}_f \leq -\rho\mathbf{T}_1^{\star T}\dot{\mathbf{q}}_1 - \mathbf{T}_2^{\star T}\dot{\mathbf{q}}_2. \quad (13)$$

Using that $\kappa_f(t) \geq 0$ and integrating (13), we have

$$\int_0^t \rho\mathbf{T}_1^{\star T}(\tau)\dot{\mathbf{q}}_1(\tau) + \mathbf{T}_2^{\star T}(\tau)\dot{\mathbf{q}}_2(\tau)d\tau \leq \kappa_f(0), \quad (14)$$

$\forall t \geq 0$. This shows that the possibly non-passive controls $(\rho\mathbf{T}_1^\star, \mathbf{T}_2^\star)$ are generated by the flywheel energy.

By designing the implementation structure (6) - (9) s.t. model uncertainties and inaccurate force measurement are totally confined in the NSD $\mathbf{\Omega}^\star(t)$ and the skew-symmetric $\Gamma(t)$, robust passivity of the closed-loop teleoperator will be guaranteed as long as the measurement of $(\dot{\mathbf{q}}_1, \dot{\mathbf{q}}_2)$ is accurate, since the NSD matrices $\mathbf{\Omega}^\star(t)$ and $\Gamma(t)$ still ensure controller passivity (10) which implies the passivity of the closed-loop teleoperator (3).

4. Robust Passivity Experiment

In this section, robust passivity is validated experimentally for the mechanical teleoperator under the control scheme proposed in [4, 5] which utilizes the passive control implementation structure (6)-(9). For more details about the control scheme, please refer to Appendix.

The proposed control law for the teleoperator achieving coordination and inertia scaling is given by:

$$\begin{pmatrix} \rho\mathbf{T}_1 \\ \mathbf{T}_2 \end{pmatrix} = \underbrace{\Gamma_d(t)\begin{pmatrix} \dot{\mathbf{q}}_1 \\ \dot{\mathbf{q}}_2 \end{pmatrix}}_{decoupling} + \underbrace{\begin{pmatrix} -\mathbf{K}_v\dot{\mathbf{q}}_E - \mathbf{K}_p\mathbf{q}_E \\ \mathbf{K}_v\dot{\mathbf{q}}_E + \mathbf{K}_p\mathbf{q}_E \end{pmatrix}}_{PD-control} + \underbrace{\begin{pmatrix} \mathbf{F}_E \\ -\mathbf{F}_E \end{pmatrix}}_{\substack{feedforward \\ cancellation}}$$
$$+ \underbrace{\frac{1-\eta}{\eta}\begin{pmatrix} \rho\mathbf{M}_1(\mathbf{q}_1) \\ \mathbf{M}_2(\mathbf{q}_2) \end{pmatrix}[\rho\mathbf{M}_1(\mathbf{q}_1) + \mathbf{M}_2(\mathbf{q}_2)]^{-1}\mathbf{F}_L}_{inertia scaling}, \quad (15)$$

(from (16), (17), (20), and (21)), where a skew-symmetric matrix $\Gamma_d(t)$ implements the decoupling control ($\mathbf{C}_{EL}, \mathbf{C}_{LE}$ in (20)-(21)), $\mathbf{q}_E = \mathbf{q}_1 - \mathbf{q}_2$, $\mathbf{K}_v, \mathbf{K}_p$ are positive definite and symmetric gains of PD-control for coordination, and $\eta > 0$ is a use-specified inertia scaling factor. Also, $\mathbf{F}_L := \rho\mathbf{F}_1 + \mathbf{F}_2$ is the total effect of the master-slave forcing on the overall motion and $\mathbf{F}_E := \phi^T(\mathbf{q})\rho\mathbf{F}_1 + [\phi^T(\mathbf{q}) - \mathbf{I}]\mathbf{F}_2$ is the mismatched forcings causing coordination error. With the potential function $V(t) := \frac{1}{2}\mathbf{q}_E^T\mathbf{K}_p\mathbf{q}_E$ and (7), we have $-\mathbf{K}_p\mathbf{q}_E = -\frac{\partial V}{\partial \mathbf{q}_1}$ and $\mathbf{K}_p\mathbf{q}_E = -\frac{\partial V}{\partial \mathbf{q}_2}$.

Since the feedforward cancellation and inertia scaling control in (15) may violate passivity, we utilize a fictitious 2-DOF flywheel. Then, we implement the feedforward cancellation, the inertia scaling control, and the damping control ($\mathbf{K}_v\dot{\mathbf{q}}_E$) as $(\rho\mathbf{T}_1^\star, \mathbf{T}_2^\star)$ in (6) and (9) via an appropriate NSD matrix $\mathbf{\Omega}^\star(t)$ s.t. (15) is duplicated as long as the flywheel energy is above a certain threshold. Here, the damping control is also implemented via (9) in order to recapture and utilize energy dissipated through the damper.

The inertia structure of the 2-DOF flywheel is designed to be diagonal ((23)) so that it has effectively 2 single-DOF flywheels. We call one the locked system flywheel (${}^LM_f$ in (23)) and the other the shape system flywheel (${}^EM_f$ in (23)). Then, the each flywheel serves as an energy reservoir to generate the each control action, exclusively, i.e. energy stored in the locked system flywheel is used to generate the inertia scaling, while the shape system flywheel energy is used for the feedforward cancellation. By utilizing this implementation structure, robust passivity is ensured as demonstrated by the following experiments.

Experimental Setup

A pair of planar 2-DOF nonlinear manipulators as shown in figure 2 is used. The master and the slave robots are equipped with force sensors that are low pass filtered at a 120Hz and a 50Hz, respectively. A control sampling rate of 500Hz is achieved. A power scaling $\rho = 15$ is used so that the human operator perceives the slave environment to be shrunk while the slave environment feels the human operator enlarged. The lengths of the two links of the master and the slave robots are $(14cm, 14cm)$ and $(38cm, 36cm)$, respectively. Therefore, the desired Cartesian *force scaling* between the master and the slave during static manipulation is around 5.7 ($\approx \rho\frac{0.14}{0.37}$), while the desired joint torque scaling is still $\rho = 15$ (i.e. $\rho\mathbf{F}_1 = \mathbf{F}_2$). Inertia scaling ($\eta = 0.6$) is used to scale down the apparent inertia of the teleoperator. Kinematic gains of the coordination control ($\mathbf{K}_v, \mathbf{K}_p$ (damping and spring) in (21)) are tuned so that coordination error of $\pm 0.5^\circ$ for both links is achieved for a position command of $\pm 140^\circ$, $0.2Hz$.

To test how the implementation structure ensures robust passivity, two levels of time delay (35ms and 350ms) are imposed on both the master and slave force sensings while

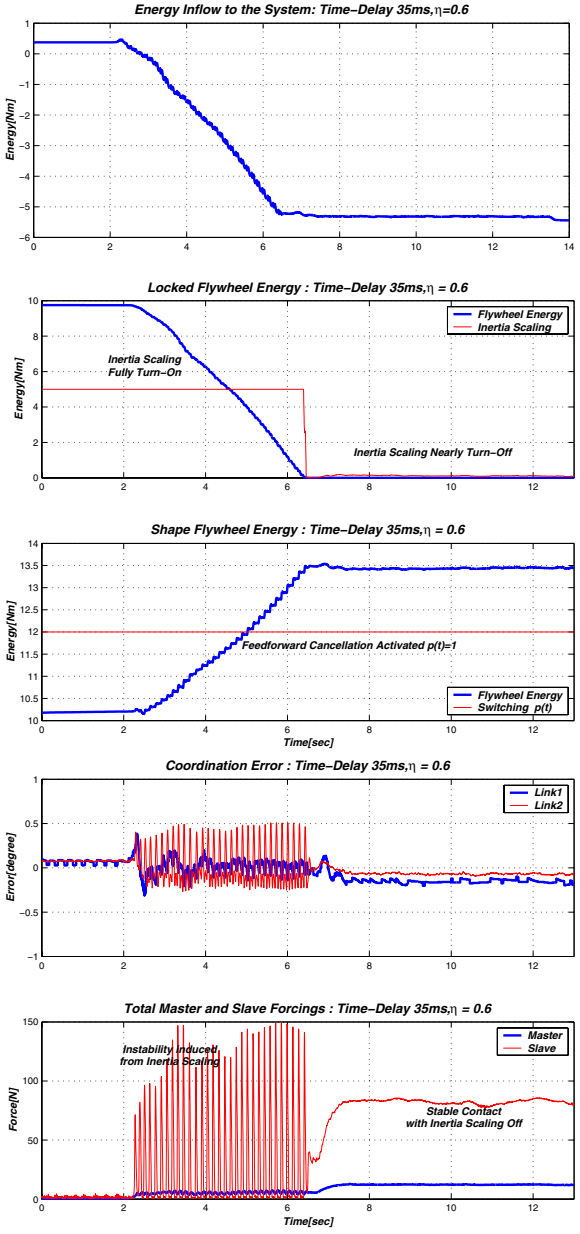

Figure 3. Plots for the robust passivity experiment with 35ms time-delay on force sensing. The locked system flywheel discharges energy to the master-slave environments (negative energy inflow) via the inertia scaling until it depletes energy so that the inertia scaling is nearly turned off and the contact becomes stable (around 6.5 sec).

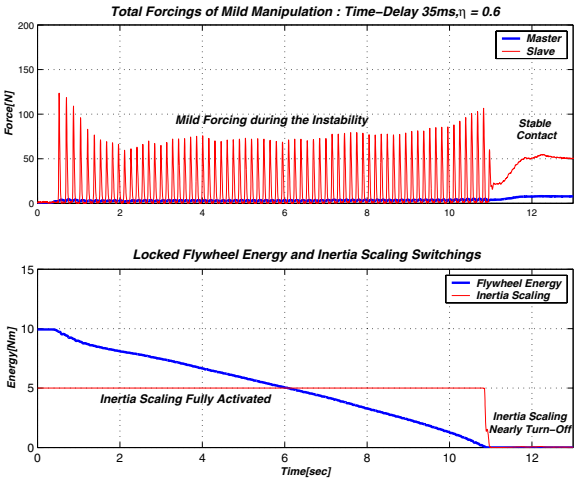

Figure 4. Plots of "mild" instability (smaller forcing) with 35ms time-delay.

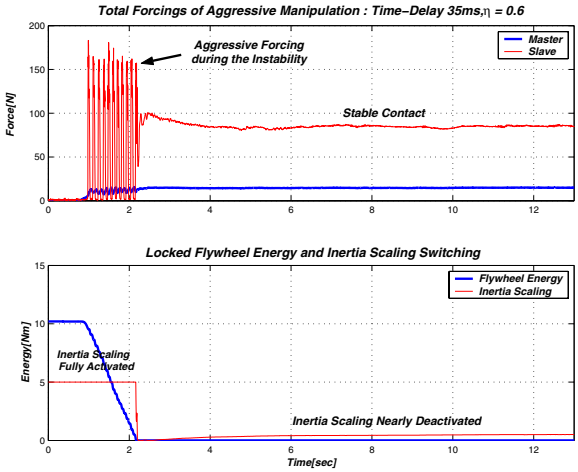

Figure 5. Plots of "aggressive" instability (larger forcing) with 35ms time-delay.

a human operator pushes (hard contact) the teleoperator on an aluminum wall of stiffness of 33kN/m installed in the slave environment.

35ms Time-Delay on Force Sensing

Figure 3 shows the result when a 35ms time-delay is imposed on the force measurement. Contact with the aluminum wall is made about 2 sec. As is envisioned by the oscillations, the time-delay induces contact instability. This is due to the inertia scaling control generated by the locked system flywheel energy. The flywheel energy decreases during the instability while the closed-loop teleoperator discharges energy to the ambient environment (the negative energy inflow). As the flywheel depletes energy below a certain threshold (around 6.5 sec), the inertia scaling control is nearly turned off. This is because the inertia scaling control proportionally decreases with the flywheel energy level, when the flywheel energy is below the threshold. Thus, the contact regains stability after 4 sec of instability. Satisfactory coordination (error less than $\pm 0.5^\circ$ for both links) is preserved during this experiment. This is because the shape system flywheel does not deplete energy so that the feedforward cancellation is turned on at all times. After the contact becomes stable (after 6.5 sec), a Cartesian force scaling of 6.4 is achieved.

In figure 4, the human operator reduces the pushing force while maintaining the instability so that the instability becomes relatively mild. Since the instability is induced by the inertia scaling control that is generated by using the locked system flywheel energy, the flywheel energy depletes only slowly so that stability is not regained until after 10 sec of instability. After the contact becomes stable again, a Cartesian force scaling of 6.2 is achieved.

In figure 5, the human operator increases the pushing force to make the instability relatively aggressive. Since this aggressive instability is induced by the inertia scaling control that is generated using the locked system flywheel energy, the flywheel depletes energy faster so that the contact becomes stable more quickly (after 1 sec of instability). A Cartesian force scaling of 5.7 is achieved afterwards. Although saturations (i.e. real forcing level is larger than that shown in figure 5) occur in the force sensing from the large forcing, passivity is still ensured due to the passive control implementation structure.

350ms Time-Delay on Force Sensing

With the 350ms time-delay (figure 6), the inertia scaling control induces instability first. Since the inertia scaling is generated using the locked system flywheel energy, the flywheel energy decreases during the instability while the closed-loop teleoperator discharges energy to the ambient environment. As the flywheel depletes energy (around 12.5 sec), the inertia scaling is nearly turned off. However, the contact remains unstable, since the feedforward cancellation starts inducing instability due to the large time-delay (after 13 sec). However, since the feedforward cancellation is generated using the shape system flywheel energy (as shown by the energy depletion of the shape system flywheel), as it depletes energy below a threshold (30 sec), the feedforward cancellation is turned off and the contact becomes stable with a Cartesian force scaling of around 6.1.

Several switchings of the feedforward cancellation in figure 6 (around 29 sec) are due to the successive re-charging (as the feedforward cancellation turned off) and depleting (as the feedforward cancellation turned-on) of the shape system flywheel energy through the damping term. After

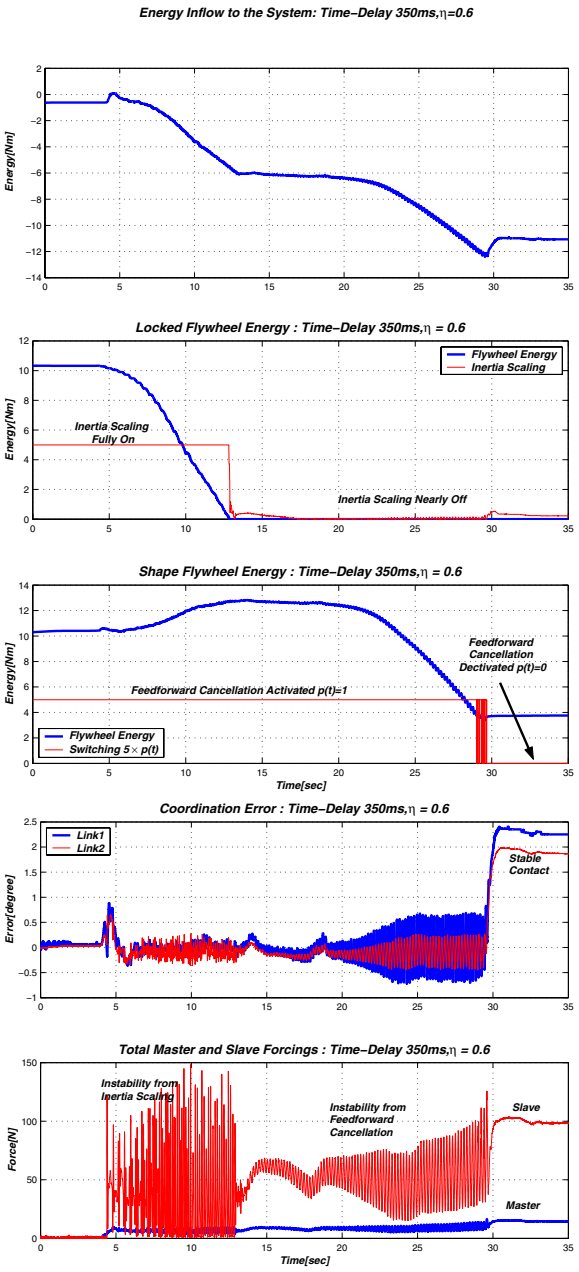

Figure 6. Plots for the robust passivity experiment with 350ms time-delay on force sensing. Instability is induced both from the inertia scaling and the feedforward cancellation due to the large time delay. The Locked and shape system flywheels discharge energy sequentially through the inertia scaling and the feedforward cancellation. As both flywheels deplete energy (13 and 30 sec), contact becomes stable eventually.

these switchings disappear, coordination degrades drastically, since the feedforward cancellation is turned off.

Discussion

This experiment clearly shows that the passive control implementation structure ensures robust passivity of the closed-loop teleoperator, i.e. the amount of the extractable energy from the closed-loop system is always bounded even in the presence of the inaccurate force sensing (with time-delay) and model uncertainties. Without the implementation structure, the instability induced from the inertia scaling control and the feedforward cancellation control would not disappear so that the amount of energy generated by the closed-loop teleoperator will be unbounded. Thus, safety and interaction stability is substantially enhanced.

In each experiment, the achieved Cartesian force scalings are slightly different (up to 12%) from the desired one (5.7) due to the calibration error of the custom-built slave force sensor which also shows slightly nonlinear hysteresis.

Notice the NSD matrix $\Omega^\star$ in (9) guarantees a negative power outflow from the controller by $\mathbf{v}^T\Omega^\star\mathbf{v} \leq 0$. This inequality is not guaranteed if the control (9) is implemented digitally so that one of $\mathbf{v}$ is hold to be constant between samples. Sufficiently fast sampling rate and some physical damping, we think, may be able to compensate for this actively generated energy by the discretization.

Under the proposed implementation structure, the closed-loop system behaves as an active system as long as the flywheels have energy. Thus, it is important to reset the flywheels when the energy builds up above a certain threshold that ensures damages on environments and operators to be acceptable while performance of the controller is reasonably preserved. For the case where the flywheel energy depletes in a very short time, saturation on the control command may be useful to avoid an extremely large control action.

5. Conclusions

In this paper, we experimentally verify that the passive control implementation structure proposed in [4, 5] ensures energetic passivity of the closed-loop teleoperator robustly, i.e. regardless of accuracy of force sensing and of model uncertainties. Experimental results show that the passive control implementation structure indeed guarantees robust passivity by limiting the amount of energy generated by the controller even in the presence of the severely corrupted force sensing (with 35ms and 350ms time-delay) and the model uncertainties. Thus, safety and interaction stability of the closed-loop teleoperator are substantially enhanced.

Appendix

A brief explanation about the control law proposed in [4, 5] is presented, which is used for the experiment in sec-

tion 4. The main innovation is the design of the transformation that decomposes the dynamics of a pair of n-DOF mechanical systems (1)-(2) into two n-DOF robot-like systems according to the two aspects of teleoperation: coordination error (shape system) and overall motion (locked system). For more information, please refer to [4, 5].

Define a decomposition matrix $\mathbf{S}(\mathbf{q})$ to be

$$\begin{pmatrix} \dot{\mathbf{q}}_L \\ \dot{\mathbf{q}}_E \end{pmatrix} = \underbrace{\begin{bmatrix} \mathbf{I} - \phi(\mathbf{q}) & \phi(\mathbf{q}) \\ \mathbf{I} & -\mathbf{I} \end{bmatrix}}_{\mathbf{S}(\mathbf{q})} \begin{pmatrix} \dot{\mathbf{q}}_1 \\ \dot{\mathbf{q}}_2 \end{pmatrix}, \qquad (16)$$

where $\phi(\mathbf{q}) := [\rho\mathbf{M}_1(\mathbf{q}_1) + \mathbf{M}_2(\mathbf{q}_2)]^{-1}\mathbf{M}_2(\mathbf{q}_2)$ and $\mathbf{q} = (\mathbf{q}_1, \mathbf{q}_2)$. $\dot{\mathbf{q}}_L$ and $\dot{\mathbf{q}}_E$ represent the velocities of the locked system (overall motion) and the shape system (coordination error). According to (16), the compatible transform for $\mathbf{T}_i, \mathbf{F}_i \quad i = 1, 2$ are:

$$\begin{pmatrix} \mathbf{T}_L \\ \mathbf{T}_E \end{pmatrix} = \mathbf{S}^{-T}(\mathbf{q}) \begin{pmatrix} \rho\mathbf{T}_1 \\ \mathbf{T}_2 \end{pmatrix}, \begin{pmatrix} \mathbf{F}_L \\ \mathbf{F}_E \end{pmatrix} = \mathbf{S}^{-T}(\mathbf{q}) \begin{pmatrix} \rho\mathbf{F}_1 \\ \mathbf{F}_2 \end{pmatrix}, \quad (17)$$

where $\mathbf{F}_L := \rho\mathbf{F}_1 + \mathbf{F}_2$ is the total effect of the master-slave forcing on the overall motion and $\mathbf{F}_E := \phi^T(\mathbf{q})\rho\mathbf{F}_1 + [\phi^T - \mathbf{I}]\mathbf{F}_2$ is the mismatched forcing causing coordination error.

Using (16)-(17), the dynamics of the teleoperator (1)-(2) are decomposed into two n-DOF robot-like systems:

$$\mathbf{M}_L(\mathbf{q})\ddot{\mathbf{q}}_L + \mathbf{C}_L(\mathbf{q}, \dot{\mathbf{q}})\dot{\mathbf{q}}_L + \mathbf{C}_{LE}(\mathbf{q}, \dot{\mathbf{q}})\dot{\mathbf{q}}_E = \mathbf{T}_L + \mathbf{F}_L \qquad (18)$$

$$\mathbf{M}_E(\mathbf{q})\ddot{\mathbf{q}}_E + \mathbf{C}_E(\mathbf{q}, \dot{\mathbf{q}})\dot{\mathbf{q}}_E + \mathbf{C}_{EL}(\mathbf{q}, \dot{\mathbf{q}})\dot{\mathbf{q}}_L = \mathbf{T}_E + \mathbf{F}_E, \qquad (19)$$

where $\mathbf{M}_L(\mathbf{q})$ and $\mathbf{M}_E(\mathbf{q})$ are symmetric and positive definite matrices, and $\mathbf{C}_{EL}(\mathbf{q}, \dot{\mathbf{q}}) + \mathbf{C}_{LE}^T(\mathbf{q}, \dot{\mathbf{q}}) = \mathbf{0}$. Remarkably, $\dot{\mathbf{M}}_L(\mathbf{q}) - 2\mathbf{C}_L(\mathbf{q}, \dot{\mathbf{q}})$ and $\dot{\mathbf{M}}_E(\mathbf{q}) - 2\mathbf{C}_E(\mathbf{q}, \dot{\mathbf{q}})$ are skew-symmetric. We call the n-DOF system (18) the *locked system*, since it represents the dynamics of the teleoperator after being perfectly coordinated (locked), whereas the n-DOF system (19) will be referred to as the *shape system* which reflects the coordination aspect (i.e. $\dot{\mathbf{q}}_E = \dot{\mathbf{q}}_1 - \dot{\mathbf{q}}_2$).

The locked and shape system controls $(\mathbf{T}_L, \mathbf{T}_E)$ are designed in [4, 5] s.t.:

$$\mathbf{T}_L = \mathbf{C}_{LE}(\mathbf{q}, \dot{\mathbf{q}})\dot{\mathbf{q}}_E + \frac{1-\eta}{\eta}\mathbf{F}_L, \qquad (20)$$

$$\mathbf{T}_E = \mathbf{C}_{EL}(\mathbf{q}, \dot{\mathbf{q}})\dot{\mathbf{q}}_L - \mathbf{K}_v\dot{\mathbf{q}}_E - \mathbf{K}_p\mathbf{q}_E - \mathbf{F}_E \qquad (21)$$

where $\eta > 0$ is a user-specified inertia scaling factor, $\mathbf{q}_E := \mathbf{q}_1 - \mathbf{q}_2$, and $\mathbf{K}_v$ and $\mathbf{K}_p$ are constant symmetric and positive definite kinematic feedback gains (damping and spring).

The shape system control (21) incorporates the feedforward cancellation of the mismatched disturbances $\mathbf{F}_E$ in (19) for the perfect coordination (i.e. $\mathbf{q}_1 = \mathbf{q}_2, \quad \forall \mathbf{F}_1, \mathbf{F}_2$) and kinematic feedback for stabilization. The locked system control (20) is for achieving the following target dynamics incorporating the inertia scaling factor $\eta > 0$ s.t.:

$$\eta\{\mathbf{M}_L(\mathbf{q})\ddot{\mathbf{q}}_L + \mathbf{C}_L(\mathbf{q}, \dot{\mathbf{q}})\dot{\mathbf{q}}_L\} = \mathbf{F}_L, \qquad (22)$$

where $\mathbf{M}_L(\mathbf{q}) = \rho\mathbf{M}_1(\mathbf{q}_1) + \mathbf{M}_2(\mathbf{q}_2))$ and $\mathbf{C}_L(\mathbf{q}, \dot{\mathbf{q}}) = \rho\mathbf{C}_1(\mathbf{q}_1, \dot{\mathbf{q}}_1) + \mathbf{C}_2(\mathbf{q}_2, \dot{\mathbf{q}}_2)$.

The designed control (20)-(21) may violate passivity due to the feedforward cancellation in (21) and the inertia scaling control in (20). Thus, the designed controls (20)-(21) are implemented in the passive control implementation structure of section 3 to ensure robust passivity of the closed-loop teleoperator. A 2-DOF fictitious flywheel is utilized as an energy storage to generate the feedforward cancellation (in (21)) and the inertia scaling control (in (20)):

$$\begin{bmatrix} {}^{L}M_f & 0 \\ 0 & {}^{E}M_f \end{bmatrix} \begin{pmatrix} {}^{L}\ddot{x}_f \\ {}^{E}\ddot{x}_f \end{pmatrix} = \begin{pmatrix} {}^{L}T_f \\ {}^{E}T_f \end{pmatrix}, \qquad (23)$$

where $({}^{L}M_f, {}^{E}M_f)$ are the (time-invariant scalar) inertia, $({}^{L}x_f, {}^{E}x_f)$ are the configuration of the flywheel, and $({}^{L}T_f, {}^{E}T_f)$ are the coupling torques to be implemented in the NSD structure (9).

Incorporating the flywheel (23), the control (20)-(21) is implemented using a NSD matrix $\mathbf{\Omega}^\star(t)$ as follows:

$$\begin{pmatrix} \mathbf{T}_L \\ \mathbf{T}_E \\ {}^{L}T_f \\ {}^{E}T_f \end{pmatrix} = \mathbf{\Omega}^\star(t) \begin{pmatrix} \dot{\mathbf{q}}_L \\ \dot{\mathbf{q}}_E \\ {}^{L}\dot{x}_f \\ {}^{E}\dot{x}_f \end{pmatrix} + \begin{pmatrix} \mathbf{0} \\ -\mathbf{K}_p\mathbf{q}_E \\ 0 \\ 0 \end{pmatrix}. \qquad (24)$$

Then, using (16) and (17), we have

$$\begin{pmatrix} \rho\mathbf{T}_1 \\ \mathbf{T}_2 \\ {}^{L}T_f \\ {}^{E}T_f \end{pmatrix} = \mathcal{S}^T(t)\mathbb{\Omega}^\star(t)\mathcal{S}(t) \begin{pmatrix} \dot{\mathbf{q}}_1 \\ \dot{\mathbf{q}}_2 \\ {}^{L}\dot{x}_f \\ {}^{E}\dot{x}_f \end{pmatrix} + \begin{pmatrix} -\mathbf{K}_p\mathbf{q}_E \\ \mathbf{K}_p\mathbf{q}_E \\ 0 \\ 0 \end{pmatrix}, \quad (25)$$

where $\mathcal{S}(t) := diag[\mathbf{S}(\mathbf{q}), \mathbf{I}]$. With a potential function $V(t) := \frac{1}{2}\mathbf{q}_E^T\mathbf{K}_p\mathbf{q}_E$, it can be shown that the implemented control (25) is exactly in the same form as (6) - (9).

Here, the NSD matrix $\mathbf{\Omega}^\star(t)$ is designed to be:

$$\mathbf{\Omega}^\star(t) := \begin{bmatrix} \mathbf{0} & \mathbf{C}_{LE}(\mathbf{q}, \dot{\mathbf{q}}) & \mathbf{\Pi}_L(t) & \mathbf{0} \\ \mathbf{C}_{EL}(\mathbf{q}, \dot{\mathbf{q}}) & \mathbf{\Delta}_d(t) & \mathbf{0} & \mathbf{\Sigma}_E(t) \\ -\mathbf{\Pi}_L^T(t) & \mathbf{0} & 0 & 0 \\ \mathbf{0} & -\mathbf{\Sigma}_E^T(t) & 0 & 0 \end{bmatrix}. \quad (26)$$

Since $\mathbf{C}_{LE}^T(\mathbf{q}, \dot{\mathbf{q}}) = -\mathbf{C}_{EL}^T(\mathbf{q}, \dot{\mathbf{q}})$ and $\mathbf{\Delta}_d(t)$ will be defined to be NSD, $\mathbf{\Omega}^\star(t)$ is indeed NSD. Main components of the matrix $\mathbf{\Omega}^\star(t)$ are:

1. Cancellation of the coupling $\mathbf{C}_{LE}(\mathbf{q}, \dot{\mathbf{q}})\dot{\mathbf{q}}_E$ and $\mathbf{C}_{EL}(\mathbf{q}, \dot{\mathbf{q}})\dot{\mathbf{q}}_L$ in (18)-(19).
2. The inertia scaling control in (20) is generated by $\mathbf{\Pi}_L(t) = \frac{1-\eta}{\eta} \cdot g({}^{L}\dot{x}_f) \cdot \mathbf{F}_L$, using the locked system flywheel energy ${}^{L}M_f$ (23), where a threshold function $g(x)$ is to ensure the controller variables in (26) to be bounded.

3. Feedforward cancellation in (21) is implemented through $\Sigma_E(t) = -g({}^E\dot{x}_f)\mathbf{K}_v\dot{\mathbf{q}}_E - \frac{p(t)}{{}^E\dot{x}_f}\mathbf{F}_E$, using the shape system flywheel energy ${}^E M_f$. Dissipated energy through $\mathbf{K}_v$ is also recaptured by this entity and stored in the shape system flywheel. Here, the threshold function $g(x)$ also ensures the controller variables in (26) to be bounded. The switching function $p(t)$ is designed in [4] to turn on/off the feedforward cancellation in (21) according to the energy level of the shape system flywheel.
4. Constant damping effect $\mathbf{K}_v$ in the shape system control (21) is achieved by $\Delta_d(t) = -\{1 - {}^E\dot{x}_f g({}^E\dot{x}_f)\}\mathbf{K}_v$ and $\Sigma_E(t)$ in the item 2 regardless of the energy level of the shape system flywheel ($|{}^E\dot{x}_f|$). However, when $|{}^E\dot{x}_f|$ is less than a threshold, some portion of energy can not be recaptured by the entity $\Sigma_E(t)$, and is dissipated through this entity which becomes negative definite.

In [4, 5], it was shown that it is possible to initialize the speed of the flywheels such that in the ideal situation (accurate force sensing and model parameters with bounded $\dot{\mathbf{q}}_1, \dot{\mathbf{q}}_2$), the energy of the flywheels will not deplete below a certain threshold. Thus, the feedforward cancellation and the inertia scaling control can be turned on all the time so that the target dynamics (22) is guaranteed.

Robust Passivity

Assume that force sensing and identified inertial parameters are inaccurate. Denote $\widehat{\star}$ as an estimate of $\star$ under this inaccuracy, then with $\widehat{\mathbf{T}}_L = \widehat{\mathbf{C}}_{LE}(\mathbf{q}, \dot{\mathbf{q}})\dot{\mathbf{q}}_E + \frac{1-\eta}{\eta}\widehat{\mathbf{F}}_L$ and $\widehat{\mathbf{T}}_E = \widehat{\mathbf{C}}_{EL}(\mathbf{q}, \dot{\mathbf{q}})\widehat{\dot{\mathbf{q}}}_L - \mathbf{K}_v\dot{\mathbf{q}}_E - \mathbf{K}_p\mathbf{q}_E - \widehat{\mathbf{F}}_E$, we have:

$$\begin{pmatrix}\widehat{\dot{\mathbf{q}}}_L \\ \dot{\mathbf{q}}_E\end{pmatrix} = \widehat{\mathbf{S}}(\mathbf{q})\begin{pmatrix}\dot{\mathbf{q}}_1 \\ \dot{\mathbf{q}}_2\end{pmatrix}, \quad \begin{pmatrix}\rho\mathbf{T}_1 \\ \mathbf{T}_2\end{pmatrix} = \widehat{\mathbf{S}}^T(\mathbf{q})\begin{pmatrix}\widehat{\mathbf{T}}_L \\ \widehat{\mathbf{T}}_E\end{pmatrix}. \quad (27)$$

Although the estimates $\widehat{\mathbf{C}}_{LE}(\mathbf{q}, \dot{\mathbf{q}})$ and $\widehat{\mathbf{C}}_{EL}(\mathbf{q}, \dot{\mathbf{q}})$ are uncertain, still $\widehat{\mathbf{C}}_{LE}(\mathbf{q}, \dot{\mathbf{q}}) = -\widehat{\mathbf{C}}^T_{EL}(\mathbf{q}, \dot{\mathbf{q}})$. Also, $\dot{\mathbf{q}}_E = \dot{\mathbf{q}}_1 - \dot{\mathbf{q}}_2$ and $\mathbf{q}_E = \mathbf{q}_1 - \mathbf{q}_2$ are always certain as long as $(\dot{\mathbf{q}}_1, \dot{\mathbf{q}}_2)$ are correct. Thus, the control using the estimates can be implemented in a similar form as (24):

$$\begin{pmatrix}\widehat{\mathbf{T}}_L \\ \widehat{\mathbf{T}}_E \\ {}^L T_f \\ {}^E T_f\end{pmatrix} = \widehat{\mathbf{\Omega}}^\star(t)\begin{pmatrix}\widehat{\dot{\mathbf{q}}}_L \\ \dot{\mathbf{q}}_E \\ {}^L\dot{x}_f \\ {}^E\dot{x}_f\end{pmatrix} + \begin{pmatrix}\mathbf{0} \\ -\mathbf{K}_p\mathbf{q}_E \\ 0 \\ 0\end{pmatrix}, \quad (28)$$

where the matrix $\widehat{\mathbf{\Omega}}^\star(t)$ is an estimate of $\mathbf{\Omega}^\star(t)$ in (26), which is still NSD. Then, using (27) and (28), it can be shown that the implementation structure is again in the same form as (25) with $\mathcal{S}^T(t)\mathbb{\Omega}^\star(t)\mathcal{S}(t)$ being replaced with $\widehat{\mathcal{S}}^T(t)\widehat{\mathbf{\Omega}}^\star(t)\widehat{\mathcal{S}}(t)$ which is still NSD. Thus, the passivity condition (12) (or the controller passivity (10)) is ensured in the presence of the model uncertainty and the inaccurate force measurement, i.e. robust passivity is achieved. However, the target dynamics may not be guaranteed, since the implemented control (28) will not duplicate the desired control (20)-(21).

References

[1] R. J. Anderson and M. W. Spong. Bilateral control of tele-operators with time delay. *IEEE Transactions on Automatic Control*, 34(5):494–501, 1989.

[2] J. E. Colgate B. Miller and R. Freeman. Guaranteed stability of haptic systems with nonlinear virtual environments. *IEEE Transactions on Robotics and Automation*, 16(6):712–719, 2000.

[3] B. Hannaford and J. Ryu. Time domain passivity control of haptic interfaces. *IEEE Transactions on Robotics and Automation*, 18(1):1–10, 2002.

[4] D. J. Lee and P. Y. Li. Passive coordination control of nonlinear bilateral teleoperated manipulators. In *Proceedings of IEEE International Conf. on Robotics and Automation*, 2002.

[5] D. J. Lee and P. Y. Li. Passive tool dynamics rendering for nonlinear bilateral teleoperated manipulators. In *Proceedings of IEEE International Conf. on Robotics and Automation*, 2002.

[6] P. Y. Li and R. Horowitz. Passive velocity field control of mechanical manipulators. In *Proceedings of the 1995 IEEE International Conf. on Robotics and Automation*, volume 3, pages 2764–2770, April 1995. Nagoya, Japan.

[7] P. Y. Li and R. Horowitz. Control of smart exercise machine: Part 1. problem formulation and non-adaptive control. *IEEE/ASME Transactions on Mechatronics*, 2(4):237–247, 1997.

[8] P. Y. Li and R. Horowitz. Passive velocity field control of mechanical manipulators. *IEEE Transactions on Robotics and Automation*, 15(4):751–763, 1999.

[9] P. Y. Li and D. J. Lee. Passive feedforward approach to bilateral teleoperated manipulators. In *Proceedings of ASME IMECE Symphosium on Haptic Interfaces for Virtual Reality and Teleoperator Systems*, 2000.

[10] P. Y. Li and Kailash Krishnaswamy. Passive bilateral teleoperation of a hydraulic acturator using an electro-hydraulic passive valve. In *Proceedings of the 2001 American Control Conference*, 2001.

[11] J. Li and P. Y. Li. Passive velocity field control (pvfc) approach to robot force control and contour following. In *Proceedings of the 2000 Japan-USA Symposium on Flexible Automation*, 1999.